Title
Scaling Shear Modulus from Small to Finite Strain for Unsaturated Soils

Journal
JOURNAL OF GEOTECHNICAL AND GEOENVIRONMENTAL ENGINEERING, 144(2)

ISSN
1090-0241

Authors
Dong, Yi
Lu, Ning
McCartney, John S

Publication Date
2018-02-01

DOI
10.1061/(ASCE)GT.1943-5606.0001819

Peer reviewed

Scaling Shear Modulus from Small to Finite Strain for Unsaturated Soils

Yi Dong, Ph.D., A.M.ASCE[1], Ning Lu, Ph.D., F.ASCE[2]

and John S. McCartney, Ph.D., P.E., M.ASCE[3]

Final submission to JGGE, March 17, 2017

[1]1Associate Professor, State Key Laboratory of Geomechanics and Geotechnical Engineering, Institute of Rock and Soil Mechanics, Chinese Academy of Sciences, Wuhan, Hubei 430071, P.R. China. Formerly, Department of Civil and Environmental Engineering, Colorado School of Mines, Golden, CO 80401, (303) 273-8663. Email: dongyi0903@gmail.com

[2]Professor, Department of Civil and Environmental Engineering, Colorado School of Mines, 1012 14th St., Golden, CO 80401. Email: ninglu@mines.edu

[3]Associate Professor, Department of Structural Engineering, University of California San Diego, La Jolla, CA 92131. Email: mccartney@eng.ucsd.edu

Abstract

The stress-dependent curve of shear modulus degradation with increasing shear strain amplitude is a fundamental mechanical property of soils. Although it is well known that the degree of saturation has an important impact on the small strain shear modulus of unsaturated soils, its role on the shear modulus evolution with strain has not been thoroughly investigated. A testing program has revealed strong correlations between two key parameters of the shear modulus degradation curve, the reference strain and the coefficient of curvature, and parameters of the soil water retention curve (SWRC). An SWRC model capable of distinguishing between soil water in the capillary and adsorption regimes was employed to correlate the reference strain to the maximum adsorption water content and pore size distribution of a soil, and to correlate the curvature coefficient to the maximum adsorption water content. A hyperbolic equation for the shear modulus reduction curve employing these correlations shows good performance in predicting the shear modulus under unsaturated small or finite strain conditions. The new model was validated using the shear modulus reduction curve of independent data sets measured at different shear strains.

Keywords: Small strain shear modulus, shear modulus reduction, bender elements, soil-water retention, suction stress, unsaturated soils.

Introduction

The degradation in shear modulus of soils with increasing shear strain amplitude has a significant impact on the design and analysis of a wide range of geotechnical engineering applications, such as deep excavations, soil-structure interaction, and the dynamic response of soils under seismic loading (Viggiani and Atkinson 1995; Kramer 1996; Rampello et al. 1997; Clayton 2011; Likitlersuang et al. 2013; Yang and Gu 2013). Experimental studies on the relationship between shear modulus reduction and shear strain have found that the strain-related shear modulus varies greatly depending on soil type, plasticity index, initial density or void ratio, stress history or over-consolidation ratio (OCR), loading cycles and frequencies, and soil degree of saturation (Hardin and Drnevich 1972a; Hardin and Drnevich 1972b; Iwasaki et al. 1978; Kokusho 1980; Yokota et al. 1981; Seed et al. 1986; Idriss 1990; Vucetic and Dobry 1991; Ishibashi and Zhang 1993; Borden et al. 1996; Darandeli 2001; Alramahi et al. 2008; Khosravi and McCartney 2012). In particular, the evolution of shear modulus with increasing shear strain amplitude for unsaturated soils is affected by both environmental loading (e.g., changes in relative humidity or matric suction) and stress state (e.g., effective stress and suction stress) (Dong et al. 2016; Dong and Lu 2016). However, the coupling between the strain-dependency of the shear modulus reduction and the hydraulic properties of unsaturated soils has not been thoroughly studied. This is partially due to the fact that several different soils that have different shear modulus reduction curves and hydraulic properties should be investigated in order to delineate correlations.

A typical strain-hardening shear stress-strain relationship of a soil is shown in Figure 1, which reflects a nonlinear increase in shear stress as the shear strains develop in the soil, with a gradual descending rate of increase until the soil reaches its peak shear strength (e.g., Viggiani and Atkinson 1995; Atkinson 2000). In other words, the ratio of shear modulus at any shear strain to the maximum shear modulus decreases with increasing shear strain. The relationship between normalized shear modulus G/G_{max} and shear strain γ is often referred to as shear modulus degradation curve or shear modulus reduction curve. When the shear strain amplitude is very small (usually less than 0.001%), the stress-strain relationship can be considered as linear elastic. In the small strain range, the shear strains in the soil primarily occur due to particle oscillation under the propagation of elastic stress waves, and do not lead to changes in the soil structure or fabric (Santamarina et al. 2001). Hence, the slope at this strain range for a given stress state can be defined as the maximum, initial, or small strain shear modulus, defined with the symbols G_{max} or G_0. On the contrary, as the shear strain increases beyond the soil-specific cyclic threshold shear strain, the soil will incur permanent deformations under static or cyclic loading. In this case, soil particles may rearrange their positions and change the numbers of contacts to adjust to the stress redistribution. Most soils will be at a strain level greater than the cyclic threshold shear strain by a shear strain of 1%, so this strain level is referred to in this study as being representative of finite strains (i.e., larger than small strains but still small with respect to strain required to reach failure in the backbone shear stress-strain curve). Accordingly, the shear modulus at this larger shear strain of 1% is referred to as the finite strain shear modulus G_1 (e.g., Lu and Kaya 2014).

Although the degradation behavior of shear modulus with increasing shear strain is well recognized, the complexities of this shear modulus degradation dependence on compaction conditions and stress states still can not be fully captured by existing models. For unsaturated soils, the mechanical properties are significantly affected by the relationships governing soil water retention and inter-particle stresses, which are coined the soil water retention curve

(SWRC) and suction stress characteristic curve (SSCC), respectively. In this study, the shear moduli at small strain levels G_{max} and finite strain levels G_l for a wide range of soils having different volumetric water contents are compared and investigated. A conceptual model previously developed by the authors is then extended to form a generalized empirical model capable of describing the strain dependency of shear modulus of unsaturated soils. The correlation between the proposed shear modulus reduction behavior and SWRC of soils reveals the effects of different regimes of soil water on patterns of shear modulus degradation for different types of soil at various degrees of saturation.

Mechanisms of Shear Modulus Strain-Dependency

Existing Shear Modulus Reduction Models

In order to describe the nonlinear shear stress-strain relationship of soils, a number of mathematical models have been proposed by different researchers to capture the features of shear modulus reduction curve. Table 1 lists four typical equations using a hyperbola to represent the shape of the curve, each containing 1 to 3 parameters. Hardin and Drnevich (1972a) introduced a reference strain γ_{ref} to normalize the already-dimensionless strain quantity for better investigation of the stress-strain behavior. The reference strain is defined as the ratio between maximum shear stress and the maximum shear modulus: $\gamma_{ref} = \tau_{max}/G_{max}$, and the shear stress-strain relationship was formulated as follows:

$$\tau = \frac{\gamma}{\frac{1}{G_{max}} + \frac{\gamma}{\tau_{max}}} = \tau_{max} \frac{\gamma}{\gamma_{ref} + \gamma} \qquad (1)$$

where τ and γ are the shear stress and shear strain, respectively. Substituting the definition of the shear modulus ($G = \tau/\gamma$), a hyperbolic equation can be further derived from Eq. 1 to represent the ratio G/G_{max} as a function of shear strain, as follows:

$$\frac{G}{G_{\max}} = \frac{1}{1+\left(\frac{\gamma}{\gamma_{\mathrm{ref}}}\right)} \quad (2)$$

In this representation, the shear modulus decreases to half of its maximum value as the shear strain increases from zero to the reference strain γ_{ref} as shown in Figure 1. However, this single-parameter model fails to fully capture the variation of the shape of the reduction curve caused by different factors such as the OCR or mean effective stress. This suggests that the reference strain varies depending on the stress state and type of soil.

To address this issue, Yokota et al. (1981) formulated an alternative expression for the modulus reduction curve that does not employ a reference strain by includes a power law function of the shear strain γ with α and β being empirical parameters, given as follows:

$$\frac{G}{G_{\max}} = \frac{1}{1+\alpha\gamma^{\beta}} \quad (3)$$

Borden et al. (1996) then modified this model by adding a third parameter to investigate the effect of cyclic loading on normalized shear modulus and damping ratio of different types of soils under various confining stresses. In the models of Yokota et al. (1981) and Borden et al. (1996), the empirically-fitted parameters lack solid physical meaning, and are difficult to determine through experimental testing programs.

Darendeli (1997, 2001) proposed a modified hyperbolic equation based on the model of Hardin and Drnevich (1972a) to quantify the shear modulus reduction curve, using the reference strain γ_{ref} and a curvature coefficient m to better represent the nonlinearity in the relationship for soils under various stress states. The model is given as follows:

$$\frac{G}{G_{\max}} = \frac{1}{1+\left(\frac{\gamma}{\gamma_{\mathrm{ref}}}\right)^{m}} \quad (4)$$

In this equation, the reference strain controls the location where G decreases to half of its maximum value as the shear strain increases, and m is a constant that represents the curvature of the modulus reduction curve. In other words, m reflects the rate of decrease in G with shear strain. This two parameter-type hyperbolic model still has a simple form with sufficient accuracy to capture the shape of the modulus reduction curve and evolution with different variables over a wide range of strain magnitudes. In the new model development, we propose a two-parameter equation building on the form of the equation of Darandeli (1997, 2001) in which the physical meaning of the parameters is investigated to consider the effect of varying initial volumetric water content of unsaturated soils.

Scaling from Small strain to Finite strain

Although the effects of mean effective stresses and OCR on the shear modulus reduction curves of saturated or dry soils have been widely explored using torsional shear or simple shear tests (e.g., Yokota et al. 1981; Ishibashi and Zhang 1993; Borden et al. 1996), fewer studies have been performed for unsaturated soils (e.g., Kim et al. 2003; Hoyos et al. 2015; Suprunenko and Ghayoomi 2015). The shear modulus degradation behavior for unsaturated soils and its dependency on soil type needs further investigation. Lu and Kaya (2014) used the drying cake method to measure the Young's modulus of soil under partially saturated conditions obtained using static loading to a shear strain of approximately 1%, and found that it is related to the volumetric water content of the soil through a power law relationship. They found that at this finite strain level, the stiffness of the material is gained from the combined stiffness of the particle and liquid components. Further, as the volumetric water content of soil decreases, the lubricating effect of water on the soil particle interaction diminishes. Dong et al. (2016) applied the relationship defined for the finite strain modulus by Kaya and Lu (2014) to the small strain shear modulus of soils to consider the impacts of the degree of saturation and the particle contact forces defined via the suction stress-based effective stress. At small strains, the stiffness of the soil skeleton arises from the stiffness of the soil skeleton due to particle hydration, and the stiffness enhanced by contact forces throughout the particle networks due to the capillarity and adsorption water, which can be characterized by the suction stress.

A schematic illustration of the mechanisms influencing the small strain and finite strain shear moduli values is shown in Figure 2. Recent advances in soil science allow a clear separation of the soil water interaction into regimes of capillary water and adsorptive water (e.g., Or and Tuller 1999; Frydman and Baker 2009; Revil and Lu 2013). Accordingly, two mechanisms attributed to the scaling effect of shear modulus variations with shear strain were proposed to represent the effect of material stiffness in soil matrix or particle clusters and the effect of contact forces. In the capillary water regime shown in Figure 2(a), the contact force is developed by the surface tension due to the presence of the air-liquid interfaces. As the water content decreases, the contact force or suction stress increases with higher curvature of the interfaces. In adsorption water regime shown in Figure 2(b), the magnitude of particle attraction due to van der Waals attraction or Coulomb forces is much higher than that due to capillary attraction (Lu and Khorshidi 2015). This indicates that the small strain shear modulus increases by a larger amount and at a greater rate than the finite strain shear modulus as the soil dries.

Following on the conceptual model in Figure 2, a modified effective stress term $\alpha \times \sigma'$ is introduced to remove the effect of stress state on the reference strain, so that the value of the reference strain in the shear modulus reduction curve can be considered as a material property that only depends on soil type and degree of saturation. This new term was incorporated into the shear modulus reduction curve of Darandeli (2001) to define a new shear modulus reduction curve as follows:

$$\frac{G}{G_{\max}} = \frac{1}{1+\left[\dfrac{\gamma}{(\alpha\sigma')\gamma_{\text{ref}}}\right]^{m}} \tag{5}$$

where α [1/kPa] is the inverse of the air-entry suction, and σ' is the mean effective stress defined using the suction stress principle, as follows:

$$\sigma' = \sigma - \sigma^{s} \tag{6}$$

where σ and σ^{s} are the mean total stress and suction stress, respectively. The values of α and σ' are related to the shape of the SWRC, which will be discussed later. It should be clarified that the parameters γ_{ref} and m in Eq. 5 are different than those in the model of Darandeli (2001) because the stress-state effects have been isolated.

Measured Soil Water Retention and Shear Modulus of Different Soils

SWRC of the Soils Tested

This study involved an investigation of several remolded soils, which were pulverized after oven dried before specimen preparation. The soil types considered range from sand, silt, to expansive clay and non-expansive clay, as listed in Table 2. Soil specimens were compacted statically using a loading frame into circular, thin cakes having a diameter of 76.2 mm and a thickness of approximately 20 mm. The matric suctions in the specimens were inferred using the transient water release and imbibition method (Wayllace and Lu 2012) for the high water content range (above ~40% degree of saturation), and the vapor adsorption isotherm technique (Likos et al. 2011) for the medium to high suction range (above ~1000 kPa). During the drying process, the evaporation rate was limited to ensure uniform water distribution within the soil cakes. The variations of sample volume were monitored by digital image analysis. Experimental details were elaborated in Lu and Kaya (2014) and Dong and Lu (2016a). Then the results of previous experimental measurements of matric suction were fitted using the new SWRC defined by Lu (2016). The SWRC of Lu (2016) can be expressed by the amount of different types of soil water in equilibrium with the soil suction or potential energy of soil water, evaluated using the following expressions:

$$\theta(\psi) = \theta_a(\psi) + \theta_c(\psi) \tag{7}$$

$$\theta_a(\psi) = \theta_a^{max}\left\{1-\left[\exp\left(1-\frac{\psi_{max}}{\psi}\right)\right]^M\right\} \tag{8}$$

$$\theta_c(\psi) = \frac{1}{2}\left[1-erf\left(\frac{\psi-\psi_{cav}}{\sqrt{2}\delta_{cav}}\right)\right]\left(\theta_s-\theta_a(\psi)\right)\left\{1+[\alpha\psi]^N\right\}^{1/N-1} \tag{9}$$

where ψ [kPa] is the matric suction, N is a pore size distribution parameter in the van Genuchten (VG) SWRC model (van Genuchten 1980), θ_a and θ_c are the volumetric water content values corresponding to the limits of the adsorptive and capillary water ranges in Figure 2, respectively. The SWRC model of Lu (2016) consists of a modified Freundlich-type model for adsorption (Eq. 8) and a VG-type model for capillarity (Eq. 9). Equations 7-9 provide a quantitative assessment of the adsorptive water by a maximum adsorption water content θ_a^{max}, and an adsorption strength parameter M. The SWRC model of Lu (2016) also introduced maximum matric suction ψ_{max}, and cavitation suction ψ_{cav} as two important controlling points to describe the soil water characteristic curves. In Eq. 9, a cumulative probability function $1/2\{1 - erf[(\psi - \psi_{cav})/(\sqrt{2}\delta_{cav})]\}$ with the standard normal distribution of the cavitation pressure $N(\psi_{cav}, \delta_{cav})$ was used to quantify the statistic uncertainty of the onset of capillary cavitation. According to Lu and Likos (2006), the suction stress can be conceptually defined as:

$$\sigma^{s}(\theta)=\sigma_{pc}^{s}(\theta)+\sigma_{c}^{s}(\theta) \quad (10)$$

where σ^{s}_{pc} is the component induced by physicochemical interaction of adsorption water (otherwise known as σ^{s}_{a}), and σ^{s}_{c} is the component induced by capillary water. Recognizing the facts that most experimental data used in this study is for matric suction within the capillary regime as the adsorptive suction stress component is not well established yet, the current study focuses on scaling of shear strain modulus within the capillary regime. Thus, the suction stress induced by matric suction in the capillary regime can be approximated by employing an effective degree of saturation concept (Lu and Likos 2006, Lu et al. 2010), and is formulated as follows:

$$\sigma^{s}\cong\sigma_{c}^{s}=-S_{e}\psi=-\frac{\theta_{c}}{\theta_{s}-\theta_{a}}\psi=-\frac{\theta-\theta_{a}}{\theta_{s}-\theta_{a}}\psi \quad (11)$$

A typical SWRC quantification of the Lu (2016) model with the separation of capillary water and adsorptive water of Hopi silt is presented in Figure 3. It is shown that the SWRC model of Lu (2016) provides an excellent fit to the sigmoidal-shape development of capillary water at medium and low suction range and the wavy behavior of adsorptive water at high suction range. The fitted results show that Hopi soil reaches a maximum matric suction of 1200 MPa with a cavitation suction of 25 MPa at the point where capillary attraction diminishes, and that Hopi silt possesses a maximum adsorption water content of 0.08. The calculated suction stress using Eq. 11 shows that Hopi silt develops suction stresses having magnitudes ranging from a few kPa at saturated conditions to approximately 100 kPa at dry conditions. The fitting parameters for all soils tested are listed in Table 2.

Comparison of G_{max} and G of the Soils Test

The finite strain shear moduli G_1 of eight tested soils were converted from their Young's moduli assuming a Poisson's ratio of 0.25 obtained from static loading tests that did not cause irreversible plastic deformation (Lu and Kaya 2014). The small strain shear moduli G_{max} of these soils were calculated from shear wave velocities measured using the bender element technique (Dong and Lu 2016a; Dong and Lu 2016b). Comparisons of the small strain and finite strain shear modulus for the 8 soils are shown in Figure 4. The general trend shows that both finite strain and small strain shear moduli increase as the water content decreases, but following different patterns. The magnitude of finite strain modulus is always lower than the small strain modulus. The overall finite strain shear modulus increases slightly from sandy soil to silty and clayey soil but generally remains less than 2 MPa. While the small strain shear modulus shows significant difference from sandy soil to silty or clayey soil. The variation of G_{max} from saturated condition to dry condition can be in the same order of magnitude with the finite strain modulus for sandy soil (e.g., 4 to 7 MPa for Esperance sand) and with little increment as soil dries. However, G_{max} for silty and clayey soil can increase in magnitude up to tens or hundreds of MPa as the soil dries (e.g., 2 to 65 MPa for Hopi silt, 18 to 257 MPa for Iowa silt, 23 to 328 MPa for Bonny silt, and 5 to 460 MPa for BALT silt). When the soil contains a higher clay content, which is reflected by the value of the maximum adsorption water content parameter, G_{max} can increase significantly from wet to dry conditions. For instance, G_{max} for Denver claystone increases up to 660 MPa as the volumetric water content decreases to 0.08. Georgia kaolinite shows an exceptional pattern from other expansive clays but resembles a similar shape of sandy soil like Esperance sand. Although G_{max} increases greatly as the Georgia kaolinite dries to a medium degree of saturation and it has significantly larger value of the modulus comparing to finite strain shear modulus, both Esperance sand and Georgia kaolinite show a plateau for degrees of saturation in the range of 0.2 to 0.8.

The above observation can be further explained by the proposed conceptual model. The stiffness of the soil matrix or particle clusters mainly contributes to the shear modulus at finite strain; while the contact force mechanism contributes to the shear modulus at small strains as the the soil dries. Capillary and adsorption water interactions play different roles in the contact force enhancement. The comparison of finite strain and small strain shear moduli of these 8 soils can be grouped into 3 categories: sandy soils with little adsorption water and relatively large pore size thus weak capillarity (e.g., Esperance sand); silty soils and expansive clayey soils with considerable amount of adsorption water and relatively small pore size hence strong capillarity (e.g., Bonny silt, Hopi silt, BALT silt, claystone); non-expansive clays which possess little adsorption water but small particle size therefore strong capillary effect (e.g., Georgia kaolinite). The contact force enhancement due to capillary results the small strain shear modulus orders of magnitude higher than finite strain shear modulus, but with fairly similar pattern. The stronger of the capillary, the more prominent of the enhancement (e.g., comparison between Esperance sand and Georgia kaolinite). The adsorption water does not contribute too much to the contact force or suction stress (Lu et al. 2010), but the crystalized water molecule structure formed by adsorptive interaction provides additional stiffness other than contact force enhancement and makes the soil matrix or material hardened. Thus, when soils dry into the adsorption water regime, the small strain shear modulus increases differently than capillary water regime, and shows more significant scaling effect comparing to the development of finite strain shear modulus in the same regime. In summary, soils containing more clay or greater fines content present stronger effects of capillarity and hydration/adsorption, therefore develop higher suction stress and show a higher small strain shear modulus.

Modulus Reduction by Strain Scaling

Once we have the finite strain and small strain shear moduli for 8 soils at various water content and the information of SWRC and SSCC for each soil, the ratio G/G_{max} can be fitted by Eq. 5. The fitting results for the three typical soil types (i.e., sandy, silty, and clayey soil) are presented in Figure 5. The left column (a-d) of the figure shows the absolute values of the shear modulus at a small shear strain of 0.0001% and at a finite strain of 1%, while the right column (e-h) of the figure shows the normalized shear modulus reduction G/G_{max} curves. Four groups of small strain and finite strain shear moduli at four different water contents for each soil were selected to demonstrate the change of the patterns and shapes of the reduction curves. The shear modulus remains more or less constant when the shear strain is less than 0.005%. Although there are only two points in this fitting process, the shape of the shear modulus reduction curve has been shown to be valid in a range of studies. Then shear moduli start to decrease around a shear strain of 0.01%, with the most significant decrease is observed between shear strains of 0.01 and 0.3%. As the shear strain increases up to approximately 1%, the shear moduli almost reach their minimum values. Throughout the comparison of three soil types, sandy soil shows relatively small magnitude of variation for shear modulus as the shear strain increases from 0.0001% to 1%. As the volumetric water content decreases from 0.26 to 0.07, the shear moduli at small strain and finite strain slightly decrease. For silty and clayey soils, the shear modulus at a shear strain of 0.0001% can increase by several orders of magnitude during drying.

The dashed line at $G/G_{max} = 0.5$ in Figure 5(e-h) reflects the positions of the reference shear strain for each shear modulus reduction curve. Comparing with the counterpart in the left column of Figure 5, the reduction curves at different water contents almost collapse into one curve, but with slightly different reference strain numbers. As the soil type changes from sandy soil to silty or clayey soil, the reference strain decreases. Specifically, for Esperance sand the reference strains are around 0.2% at saturation and slightly increases as soil dries; for Hopi silt the reference shear strains are around 0.1% at saturation and the values oscillate back and forth as the soil dries; for Iowa silt or Denver claystone the reference strains are decreasing as the soils dry, and apparently their reference strains vary in a wider range comparing to those of Hopi silt and Esperance sand. This observation suggests that the reference strain of a certain soil is not always a constant number under unsaturated conditions, and its value varies from soil to soil and changes depends on the volumetric water content and porosity. The collapse of the different reduction curves into one normalized reduction curve from the left to right columns indicates that the coefficient of curvature *m* might be constant for each soil at various volumetric water contents but may alter depending on the soil type.

Correlation Between G/G_{max} and SWRC Parameters

The analysis in the previous section leads to an examination of the dependencies of the reference strain γ_{ref} and coefficient of curvature *m*, on volumetric water content for each soil type. The relationships between reference strain and volumetric water content are shown in Figure 6(a), while the relationships between coefficient of curvature and volumetric water content are shown in Figure 6(b) for sandy, silty, and clayey soils. The results in Figure 6 further confirm the intuitive assessment on the characteristics of reference strain and coefficient of curvature and quantifies the dependencies of these two parameters on water content for each soil.

In the case of sandy soils (e.g., Esperance sand), the reference strain is almost one order of magnitude higher than that of the silty and clayey soils. Additionally, Esperance sand exhibits an opposite pattern of evolution with water content comparing to other silty soils and clayey soils. This is possibly related to the suction stress evolution at varying volumetric water content for sandy soil, where suction stress first increases then decreases as the sample dries from saturation.

Esperance sand has the largest reference strain at dry condition than at wet condition; while Hopi silt and BALT silt show monotonically increases in reference strain with increasing volumetric water content; and claystone presents a larger increment as the volumetric water content increases comparing to the other soils. Generally, the reference strain and the volumetric water content are found to be related by a power law relationship, as follows:

$$\gamma_{\mathrm{ref}} = \eta \times (\theta^{\xi}) \tag{12}$$

where η is a multiplier parameter and ξ is the power of water content. These two parameters indicate the range or extent of reference strain variation with water content. The trend lines in Figure 6a show a good fit for each soil with a correlation coefficient R^2 higher than 0.96.

The relationships between the curvature coefficient m and volumetric water content for each selected soil are presented in Figure 6(d-f). It is shown that the values of m are mainly unchanged, indicating that there is no dependency on the volumetric water content for this parameter. The overall number of m ranges from 1.0 to 2.0 for different soils. In light of this feature of m evolution with θ, it is considered that for a certain type of soil the curvature coefficient is a constant, but it varies depending on soil type. Accordingly, a mean value was taken for each soil averaging over the different volumetric water contents.

After the determination of the dependency of reference strain on volumetric water content, and the averaged curvature coefficient over various volumetric water contents for each soil, the correlations between parameters ξ, η, and averaged m and the known parameters of the SWRC for each soil are summarized in Figure 7. The parameters of the SWRC model of Lu (2016) were obtained by fitting the measured matric suctions as shown in Figure 3. The numbers of all fitted parameters are listed in Table 2. The correlations between water content-dependent parameters of reference strain (ξ and η) were investigated over all SWRC parameters (i.e., α, N, θ_a^{max}, M).

Figure 7(a-b) show selected correlation between ξ and N, and correlation between ξ and α. It can be considered that parameter ξ has a strong linear relationship with the pore size distribution parameter N, while no obvious trend can be found between ξ and other SWRC parameters. Hence, an empirical equation can be used to connect the parameter ξ with the SWRC parameter N, as follows:

$$\xi = -3.0 \times N + 6.9 \tag{13}$$

This equation suggests that a higher N value corresponds to lower ξ value, implying that a more prominent variation of reference strain with volumetric water content occurs in clayey or silty soil with lower N value, while less change in reference strain with volumetric water content occurs in sandy soil with a higher N value. This is consistent with the results shown in Figure 6(a-d) and Figure 7(a-c).

Similarly, parameter η was investigated by trials of correlating η to all SWRC parameters, and a linear relationship between η and maximum adsorption water θ_a^{max} was observed as shown in Figure 7c. An empirical fitting equation is formulated as follows:

$$\eta = 0.10 \times \theta_a^{max} \tag{14}$$

As an indicator of the reference strain variation, Eq. 14 indicates that parameter η increases linearly with θ_a^{max}, implying that soils with higher θ_a^{max} tend to have a larger variation in the reference strain. Together with the relationship for the parameter ξ, the correlation between η and θ_a^{max} leads to the conclusion that silty or clayey soils with higher fines contents will show greater variations in the reference strain as the volumetric water content changes. This also confirms the observations from Figure 6(a-d) and Figure 7(a-c).

The curvature coefficient m can be assumed as a soil-type dependent parameter insensitive to changes in volumetric water content. The correlation between m and the SWRC parameters shows a connection between the extent of shear modulus degradation and the maximum adsorption water content in soil. The correlation observed in Figure 7e can be captured by the following expression:

$$m = 0.25 \times \ln(\theta_a^{max}) + 2.34 \tag{15}$$

The curvature coefficient shows a logarithmic relationship with increasing maximum adsorption water content. This correlation reveals that the amount of adsorption water in the fines content of a givne soil directly influences the degradation rate of shear modulus from small strain to finite strain levels. It also reflects that the higher adsorption water content results in larger difference in orders of magnitude between small strain shear modulus and finite strain shear modulus. This trend, again, proves the contact-force mechanism of the conceptual model that when soil contains more clay content, more significant enhancement of shear modulus prevails at small strain. In the case of zero mean total stress, this enhancement also can be characterized by the evolution in suction stress during drying of a soil (Dong and Lu 2016a).

Prediction and Validation of Shear Modulus

The correlations among the shear modulus reduction parameters (i.e., ξ, η and m) and the Lu (2016) SWRC model parameters (i.e., N and θ_a^{max}), provide a convenient approach to estimate either the small strain or finite strain moduli of a soil in the case that one or the other is given and the SWRC of the soil is known. By substituting Eqs. 13 and 14 into Eq. 12, then substituting Eqs. 12 and 15 into Eq. 5, the following predictive equation for the normalized shear modulus reduction curve can be defined:

$$\frac{G}{G_{max}} = \frac{1}{1 + \left[\dfrac{\gamma}{\alpha \sigma' \left(0.10\theta_a^{max}\right) \theta^{-3.0n+6.9}} \right]^{0.25\ln\left(\theta_a^{max}\right)+2.34}} \tag{16}$$

This equation establishes an approach of determining the normalized shear modulus reduction curve for soils under unsaturated conditions by using empirical correlations based on the SWRC and volumetric water content. Knowing the SWRC information for a certain soil, the small strain shear modulus can be predicted from the finite strain shear modulus, or the other way around. The performance of Eq. 16 is presented in Figure 8. For both predicting small strain or finite strain moduli values, the predicted data points are mainly distributed along the 1:1 diagonal line with small scattering with respect to the measured ones. The R^2 values show a good estimation using the proposed model.

Another validation of the prediction was performed using shear modulus reduction data for 3 other unsaturated soils available in the literature. The SWRC parameters was obtained by fitting the experimental SWRC measurements of a silty sand from Hoyos et al. (2015), a subgrade soil from Kim et al. (2003), and Ottawa F75 sand from Suprunenko and Ghayoomi (2015), with the SWRC model of Lu (2016), as shown in Figures 9(a, c, and e), respectively. The predictions of shear modulus at different strain levels were then compared with experimental data obtained from different cyclic loading tests and resonant column tests, as shown in Figures 9(b, d, and e). The silty sand sample were tested under a net confining pressure of 25 kPa and two different suction values (a suction of 25 kPa corresponding to a volumetric water content of $\theta = 0.29$, and a suction of 200 kPa corresponding to a volumetric water content of $\theta = 0.17$). The subgrade soil was tested under an effective confining pressure of 41 kPa and various suctions (i.e., 5, 20, 50, 100, and 200 kPa). The Ottawa sand was tested under an effective confining stress of 50 kPa and a suction of 3 kPa. The soils have adsorptive water contents ranging from 0.009 to 0.075, and pore size spectrum parameter N values ranging from 1.436 to 2.525. It is shown that the predicted curves generally compare well with the measured data points. The different predictions of the shear modulus reduction curves show a good match with the positions of the reference strain, the overall curvature of the degradation curve, and the variation of reduction curve under different suction values. The predicted curves were found to slightly overestimate or underestimate the shear modulus at small and finite strain values, the deviation can be considered acceptable indicating a reliable prediction. Uncertainties may arise from the experimental measurements of resonant column test or torsional shear test. Some extra work measuring a complete SWRC especially in the high suction range is necessary to obtain good predictions of the shear modulus reduction.

Summary and Conclusions

In this paper, the small strain shear moduli and finite strain shear moduli were compared to evaluate the different mechanisms governing the shear modulus reduction with increasing shear strain amplitude. It was found that the shear modulus at finite strains is controlled by the soil structure, while the shear modulus at small strains is controlled by inter-particle contact forces associated with the pore water in the capillarity or adsorption regimes. The SWRC model of Lu (2016) clearly distinguishes between the capillary and adsorption soil water regimes, which helped to better interpret the impacts of soil type and volumetric water content on the shear modulus reduction curve.

Using the results from tests on 8 different soil types (ranging from sandy, silty, to clayey soils), a new shear modulus reduction curve was established to take into consideration of the dependency of water content and the effect of soil water adsorption. Relationships between key parameters of this model, the reference strain and curvature coefficient, were defined based on the results from the experimental testing program. The reference strain was found to be in a power law relationship with water content for a certain soil, with a magnitude varying from soil to soil. The curvature coefficient is soil-type dependent and was not as sensitive to the volumetric water content. Using the SWRC model of Lu (2016), the reference strain was correlated with the maximum adsorption water content and the pore spectrum indicator of the SWRC. The curvature coefficient reflected the effect of soil water hydration, and is found to be correlated with soil water adsorption. The proposed prediction approach provides a simple and convenient equation to estimate either small strain or finite strain shear modulus by knowing one of the other and the information of soil water retention. It also can be used to calculate the shear modulus of a soil at any given strain level by knowing the SWRC and the maximum shear modulus.

Acknowledgements

This research is supported by a grant from the National Science Foundation (NSF CMMI-1230544). The authors also would like to thank L. Hoyos of the University of Texas at Arlington for the private correspondence regarding the unpublished experimental data.

References

Alramahi, B., Alshibli, K., Fratta, D., and Trautwein, S. (2008). “A suction-control apparatus for the measurement of p and s-wave velocity in soils.” *Geotechnical Testing Journal*, *31*(1), 471.

Atkinson, J. H. (2000). “Non-linear soil stiffness in routine design.” *Géotechnique*, 50(5), 487–508.

Borden, R. H., Shao, L., and Gupta, A. (1996). “Dynamic properties of Piedmont residual soils.” *Journal of geotechnical engineering ASCE*, 122(10), 813–821.

Clayton, C.R.I. (2011). “Stiffness at small strain: research and practice.” *Géotechnique*, 61(1), 5–37.

Cho, G.C., and Santamarina, J.C. (2001). “Unsaturated particulate materials: particle-level studies.” *Journal of Geotechnical and Geoenvironmental Engineering*, 127(1):84–96.

Darendeli, M. B., (1997). “Dynamic properties of soils subjected to 1994 Northridge earthquake.” M.S. Thesis, University of Texas at Austin.

Darendeli, M. B., (2001). “Development of a new family of normalized modulus reduction and material damping curves.” Ph.D. Thesis, University of Texas at Austin.

Dong, Y., Lu, N., Wayllace, A., and Smits, K. (2014). “Measurement of thermal conductivity function of unsaturated soil using a transient water release and imbibition method.” *Geotechnical Testing Journal*, 37(6), 980–990.

Dong, Y., and Lu, N., (2016a). “Correlation between small strain shear modulus and suction stress of unsaturated soils in capillary regime.” *Journal of Geotechnical and Geoenvironmental Engineering*, in print.

Dong, Y., and Lu, N., (2016b). "Dependencies of Shear Wave Velocity and Shear Modulus of Soil on Saturation." *Journal of Engineering Mechanics*, in print.

Dong, Y., Lu, N., and McCartney, J.S. (2016). "A unified model for small strain shear modulus of variably saturated soil." *Journal of Geotechnical and Geoenvironmental Engineering*.

Fredlund, D. G., and Xing, A. (1994) "Equations for the soil-water characteristic curve." *Canadian Geotechnical Journal,* 31(4) (1994): 521–532.

Frydman, S., and Baker, R. (2009). "Theoretical soil-water characteristic curves based on adsorption, cavitation, and a double porosity model." *International Journal of Geomechanics*, 9(6), 250–257.

Hardin B.O., and Richart F.E. (1963). "Elastic wave velocities in granular soils." *Journal of Soil Mechanics and Foundations Division ASCE,* 89(1):33–65.

Hardin B.O., and Drnevich V.P. (1972a). "Shear modulus and damping in soils: measurement and parameter effects." *Journal of Soil Mechanics and Foundations Division ASCE,* 98(SM6), 603–624.

Hardin B.O., and Drnevich V.P. (1972b). "Shear modulus and damping in soils: design equations and curves." *Journal of Soil Mechanics and Foundations Division ASCE,* 98(SM7), 667–692.

Heitor A., Indraratna B., and Rujikiatkamjorn C. (2013). "Laboratory study of small strain behavior of a compacted silty sand." *Canadian Geotechnical Journal*, 50(2), 179–188.

Hoyos, L. R., Suescún-Florez, E. A., and Puppala, A. J. (2015). "Stiffness of intermediate unsaturated soil from simultaneous suction-controlled resonant column and bender element testing." *Engineering Geology*, 188, 10–28.

Idriss, I. M. (1990). "Response of soft soil sites during earthquakes." *Proceedings, H. Bolten Seed Memorial Symposium*, 2, 273–298.

Ishibashi, I., and Zhang, X. (1993). "Unified dynamic shear moduli and damping ratio of sand and clay." *Soils and Foundations*, 33(1), 182–191.

Iwasaki, T., Tatsuoka, F., and Takagi, Y. (1978). "Shear moduli of sands under cyclic torsional shear loading." *Soils and Foundations*, 18(1), 39–56.

Jackson, R.D., Reginato, R.J., and Van Bavel, C.H.M. (1965). "Comparison of measured and calculated hydraulic conductivities of unsaturated soils." *Water Resources Research,* 1(3), 375–380.

Khosravi, A., and McCartney, J.S. (2012). "Impact of hydraulic hysteresis on the small strain shear modulus of low plasticity soils." *Journal of Geotechnical and Geoenvironmental Engineering*, 138(11), 1326–1333.

Kim, D.S., Seo, W.S., and Kim, M.J. (2003) "Deformation characteristics of soils with variations of capillary pressure and water content." *Soils and Foundations*, 43(4), 71–79.

Kokusho, T. (1980). "Cyclic triaxial test of dynamic soil properties for wide strain range." *Soils and Foundations*, 20(2), 45–60.

Kramer, S.L. (1996). "*Geotechnical Earthquake Engineering*." Prentice Hall, Upper Saddle River, NJ.

Lebeau, M., and Konrad, J.M. (2010). "A new capillary and thin film flow model for predicting the hydraulic conductivity of unsaturated porous media." *Water Resources Res*earch, 46, W12554.

Likitlersuang, S., Teachavorasinskun, S., Surarak, C., Oh, E. and Balasubramaniam, A. (2013). "Small strain stiffness and stiffness degradation curve of Bangkok clays." *Soils and Foundations*, 53(4), 498–509.

Likos, W. J., Lu, N., and Wenszel, W. (2011) "Performance of a dynamic dew point method for moisture isotherms of clays." *Geotechnical Testing Journal*, 34(4), 373–382.

Lu, N. (2016). "Generalized Soil Water Retention Equation for Adsorption and Capillarity." *Journal of Geotechnical and Geoenvironmental Engineering*, in print.

Lu, N., and Khorshidi, M. (2015). "Mechanism for soil-water retention and hysteresis at high suction range." *Journal of Geotechnical and Geoenvironmental Engineering*, 141(8), 04015032.

Lu, N., Godt, J., and Wu, D. (2010). "A closed form equation for effective stress in variably saturated soil." *Water Resources Research*, 46(5), W05515.

Lu, N., and Kaya, M. (2013). "A drying cake method for measuring suction-stress characteristic curve, soil-water-retention curve, and hydraulic conductivity function." *Geotechnical Testing Journal*, 36(1), 1–19.

Lu, N. (2008). "Is matric suction a stress variable?" *Journal of Geotechnical and Geoenvironmental Engineering*, 134(7), 899–905.

Lu, N., and Likos, W.J. (2006). "Suction stress characteristic curve for unsaturated soils." *Journal of Geotechnical and Geoenvironmental Engineering*, 132(2), 131–142.

Lu, N., and Likos, W.J. (2004). "*Unsaturated Soil Mechanics*." Wiley, Hoboken, NJ.

Mendoza, C.E., Colmenares, J.E., and Merchán, V.E., (2005), "Stiffness of an unsaturated compacted clayey soil at very small strains." In: *Proceedings of international symposium* *on advanced experimental unsaturated soil mechanics*, 27–29 June, Trento, Italy, pp 199–204.

Oh, W.T., and Vanapalli, S.K., (2014). "Semi-empirical model for estimating the small strain shear modulus of unsaturated non-plastic sandy soils." *Geotechnical and Geological Engineering*, 32, 259–271.

Or, D., and Tuller, M. (1999). "Liquid retention and interfacial area in variably saturated porous media: upscaling from single-pore to sample-scale model." *Water Resources Research*, 35, 3591–3605.

Rampello, S., Viggiani, G. M. B., and Amorosi, A. (1997). "Small-strain stiffness of reconstituted clay compressed along constant triaxial effective stress ratio paths." *Géotechnique*, 47(3), 475–489.

Revil, A., and Lu, N. (2013). "Unified water sorption and desorption isotherms for clayey porous materials." *Water Resources Research*, 49(9), 5685–5699.

Santamarina, J.C., Klein, K.A., and Fam, M.A. (2001). "*Soils and Waves: Particulate Materials Behavior, Characterization and Process Monitoring*," Wiley, Chichester, U.K.

Sawangsuriya, A., Edil, T.B., and Bosscher, P.J. (2009). "Modulus-suction moisture relationship for compacted soils in post compaction state." *Journal of Geotechnical and Geoenvironmental Engineering*, 135(10), 1390–1403.

Seed, H.B., Wong, R.T., Idriss, I.M. and Tokimatsu, K. (1986). "Moduli and damping factors for dynamic analyses of cohesionless soils." *Journal of Geotechnical Engineering*, 112(11), 1016–1032.

Shibuya, S., and Mitachi, T. (1994). "Small strain shear modulus of clay sedimentation in a state of normal consolidation." *Soils and Foundations*, 34(4), 67–77.

Sorensen, K.K., Baudet, B.A., and Simpson, B. (2010). "Influence of strain rate and acceleration on the behaviour of reconstituted clays at small strains." *Géotechnique*, 60(10), 751–763.

Suprunenko, G. and Ghayoomi, M. (2015). "Suction-Controlled Cyclic Triaxial System for Measurement of Dynamic Properties of Unsaturated Soils", XV Pan-American Conference on Soil Mechanics and Geotechnical Engineering, Buenos Aires, Argentina, 2150–2157.

Truong, Q., Lee, J., Dong, Y., and Yun, T. (2011). "Capillary induced small strain stiffness for hydrophilic and hydrophobic granular materials: Experimental and numerical studies." *Soils and Foundations*, 51(4), 713–721.

Tuller, M., Or, D., and M.Dudley, L., (1999). "Adsorption and capillary condensation in porous media-liquid retention and interfacial configurations in angular pores." *Water Resources Research*, 35(7), 1949–1964.

Tuller, M., and Or, D., (2005). "Water films and scaling of soil characteristic curves at low water contents." *Water Resources Res*earch, 41, W09403.

van Genuchten, M.T. (1980). "A closed-form equation for predicting the hydraulic conductivity of unsaturated soils." *Soil Science Society of America Journal*, 44(5), 892–898.

Viggiani, G., and Atkinson, J. H. (1995). "Stiffness of fine-grained soil at very small strains." *Géotechnique*, 45(2), 249–265.

Vucetic, M. and Dobry, R. (1991). "Effect of soil plasticity on cyclic response." *Journal of Geotechncial Engineering ASCE*, 117(1), 89–107.

Yang, J. and Gu, X.Q. (2013). "Shear stiffness of granular material at small strains: does it depend on grain size?" *Géotechnique*, 63(2), 165–179.

Yokota, K., Imai, T., and Konno, M. (1981). "Dynamic deformation characteristics of soils determined by laboratory tests". *OYO Tec. Rep*, 3, 13–37.

Wayllace, A., and Lu, N. (2012). "A transient water release and imbibitions method for rapidly measuring wetting and drying soil water retention and hydraulic conductivity functions." *Geotechnical Testing Journal*, 35(1), 1–15.

List of Tables and Figures

Table 1

Reference	Model	Parameters
Hardin and Drnevich (1972a)	$\frac{G}{G_{\max}}=\frac{1}{1+\frac{\gamma}{\gamma_{\mathrm{ref}}}}$	γ_{ref}
Yokota et al. (1981)	$\frac{G}{G_{\max}}=\frac{1}{1+\alpha\cdot\gamma^{\beta}}$	α and β
Borden et al. (1996)	$\frac{G}{G_{\max}}=\frac{1}{\left(1+a\cdot\gamma^{b}\right)^{c}}$	a, b, and c
Darandeli (2001)	$\frac{G}{G_{\max}}=\frac{1}{1+\left(\frac{\gamma}{\gamma_{\mathrm{ref}}}\right)^{m}}$	γ_{ref} and m

Table 2

No.	Soil	USCS	Porosity	Correlation			Lu SWRC model parameters			
			ϕ	m	ξ	η	α	N	θ_a^{max}	M
1*	Esperance sand	SP	0.39	1.141	-0.342	0.0026	0.220	2.520	0.010	0.009
2*	Bonny silt	ML	0.47	1.423	1.857	0.0027	0.091	1.531	0.024	0.058
3*	Hopi silt	SC	0.48	1.513	1.416	0.0059	0.046	1.742	0.063	0.122
4*	BALT silt	ML	0.47	1.580	2.086	0.0028	0.059	1.726	0.024	0.127
5*	Iowa silt	ML	0.45	1.609	1.195	0.0067	0.083	1.654	0.046	0.101
6*	Denver claystone	CL	0.55	1.656	2.974	0.0113	0.010	1.560	0.111	0.076
7*	Denver bentonite	CH	0.53	1.997	3.063	0.0159	0.014	1.410	0.156	0.196
8*	Georgia kaolinite	CL	0.58	1.762	-0.301	0.0082	0.011	2.350	0.070	0.010
9#	Silty sand	SM	0.42	1.705	2.612	0.0081	0.058	1.436	0.075	0.033
10†	Subgrade soil	SP	0.40	1.183	0.766	0.0019	0.015	2.056	0.009	0.007
11‡	Ottawa F75	SW	0.30	1.339	-0.630	0.0027	0.214	2.525	0.017	0.003

* data from Dong and Lu (2016a), test conducted by using drying and wetting cake technique;
# data from Hoyos et al. (2015), test conducted by suction-controlled resonant column technique;
† data from Kim et al. (2003), test conducted in a torsional resonant column system;
‡ Data from Suprunenko and Ghayoomi (2015), measured in a strain-controlled cyclic triaxial testing device.

Figure 1

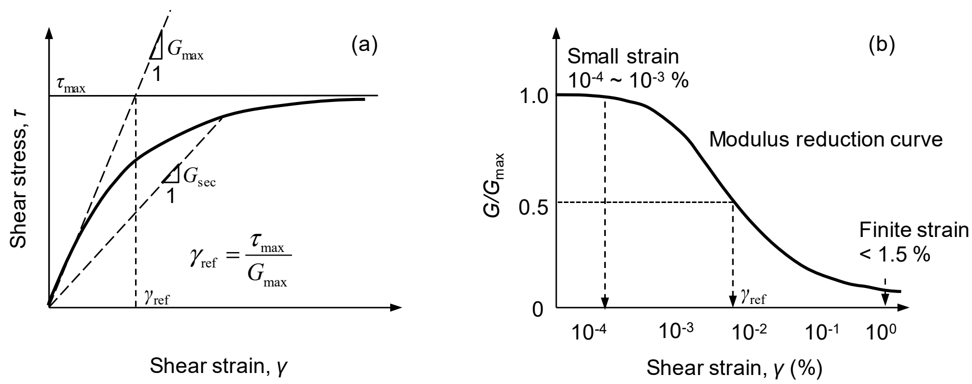

(a)
$G_{\max}$
1
$\tau_{\max}$
$G_{\sec}$
1
Shear stress, τ
$\gamma_{\mathrm{ref}} = \frac{\tau_{\max}}{G_{\max}}$
γ_{ref}
Shear strain, γ
(b)
Small strain
10^{-4} ~ 10^{-3} %
1.0
Modulus reduction curve
$G/G_{\max}$
0.5
Finite strain
< 1.5 %
0
γ_{ref}
10^{-4}
10^{-3}
10^{-2}
10^{-1}
10^{0}
Shear strain, γ (%)

Figure 2

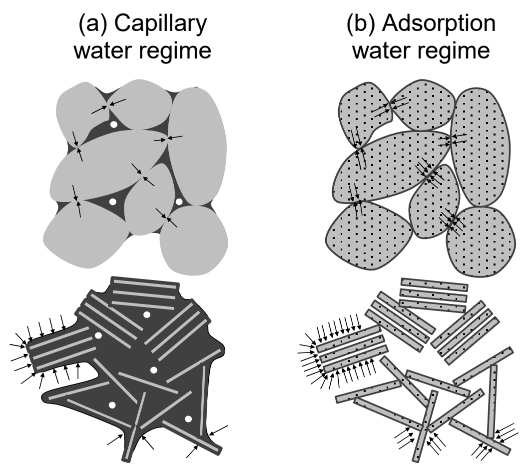

Figure 3

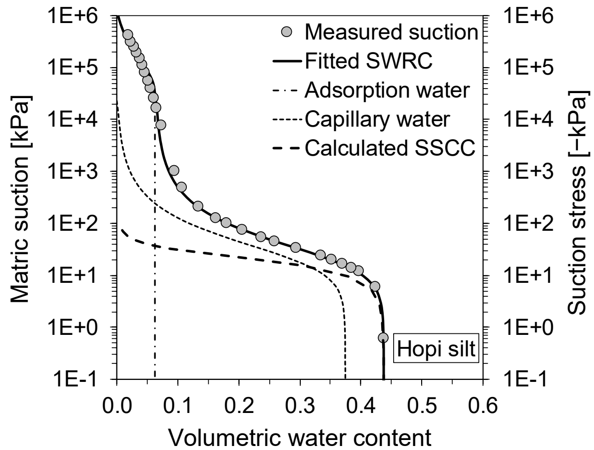

Measured suction
Fitted SWRC
Adsorption water
Capillary water
Calculated SSCC
Hopi silt
Matric suction [kPa]
Suction stress [−kPa]
Volumetric water content
1E+6
1E+5
1E+4
1E+3
1E+2
1E+1
1E+0
1E-1
0.0
0.1
0.2
0.3
0.4
0.5
0.6

Figure 4

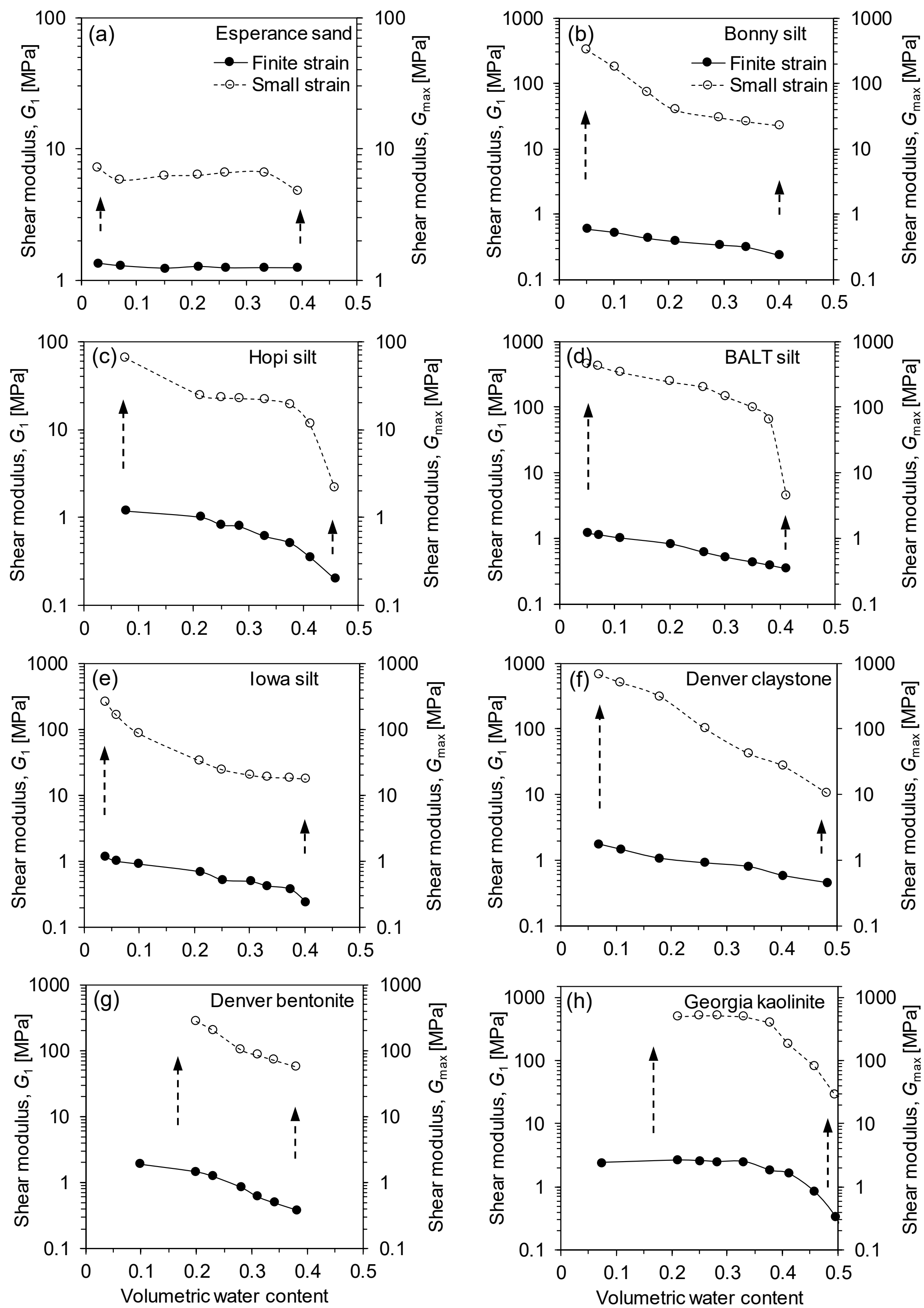

(a) Esperance sand
(b) Bonny silt
(c) Hopi silt
(d) BALT silt
(e) Iowa silt
(f) Denver claystone
(g) Denver bentonite
(h) Georgia kaolinite
Finite strain
Small strain
Shear modulus, G_1 [MPa]
Shear modulus, G_{max} [MPa]
Volumetric water content

Figure 5

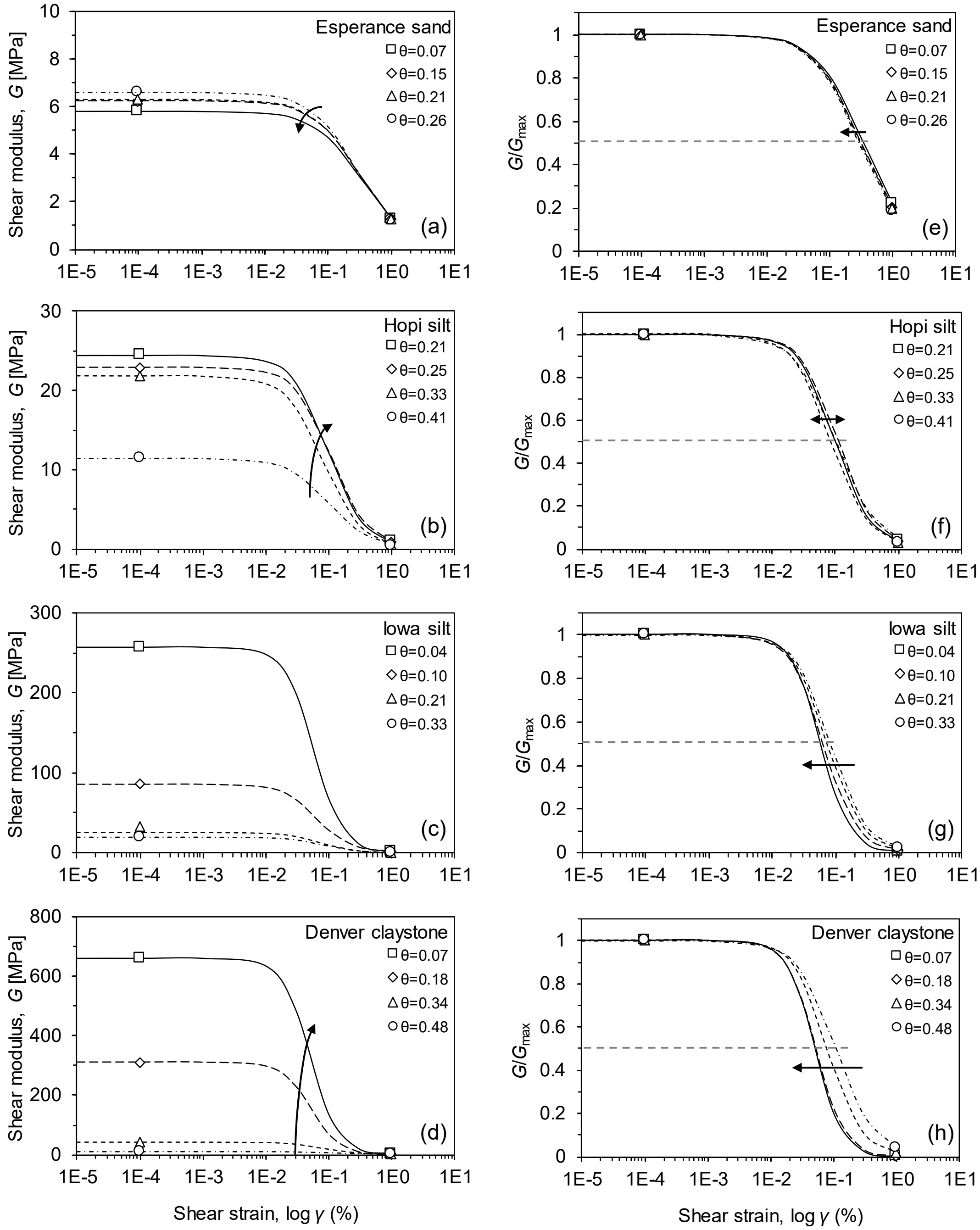
Esperance sand
θ=0.07
θ=0.15
θ=0.21
θ=0.26
(a)
(e)
Hopi silt
θ=0.21
θ=0.25
θ=0.33
θ=0.41
(b)
(f)
Iowa silt
θ=0.04
θ=0.10
θ=0.21
θ=0.33
(c)
(g)
Denver claystone
θ=0.07
θ=0.18
θ=0.34
θ=0.48
(d)
(h)
Shear modulus, G [MPa]
G/Gmax
Shear strain, log γ (%)

Figure 6

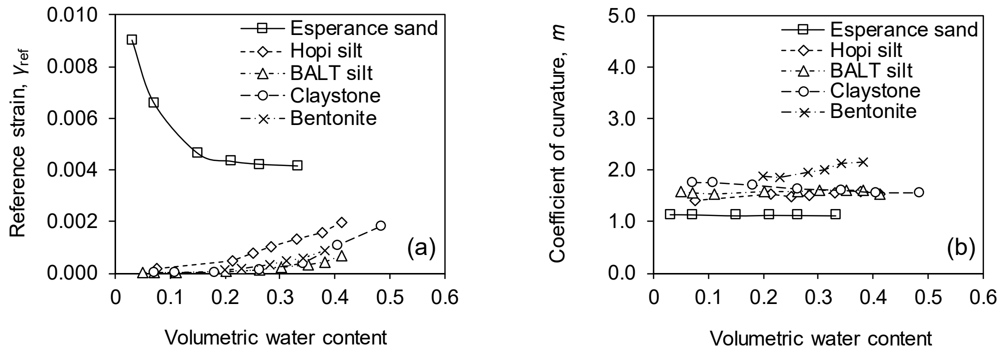

0.010
0.008
0.006
0.004
0.002
0.000
Reference strain, γref
Esperance sand
Hopi silt
BALT silt
Claystone
Bentonite
(a)
0
0.1
0.2
0.3
0.4
0.5
0.6
Volumetric water content
5.0
4.0
3.0
2.0
1.0
0.0
Coefficient of curvature, m
Esperance sand
Hopi silt
BALT silt
Claystone
Bentonite
(b)
0
0.1
0.2
0.3
0.4
0.5
0.6
Volumetric water content

Figure 7

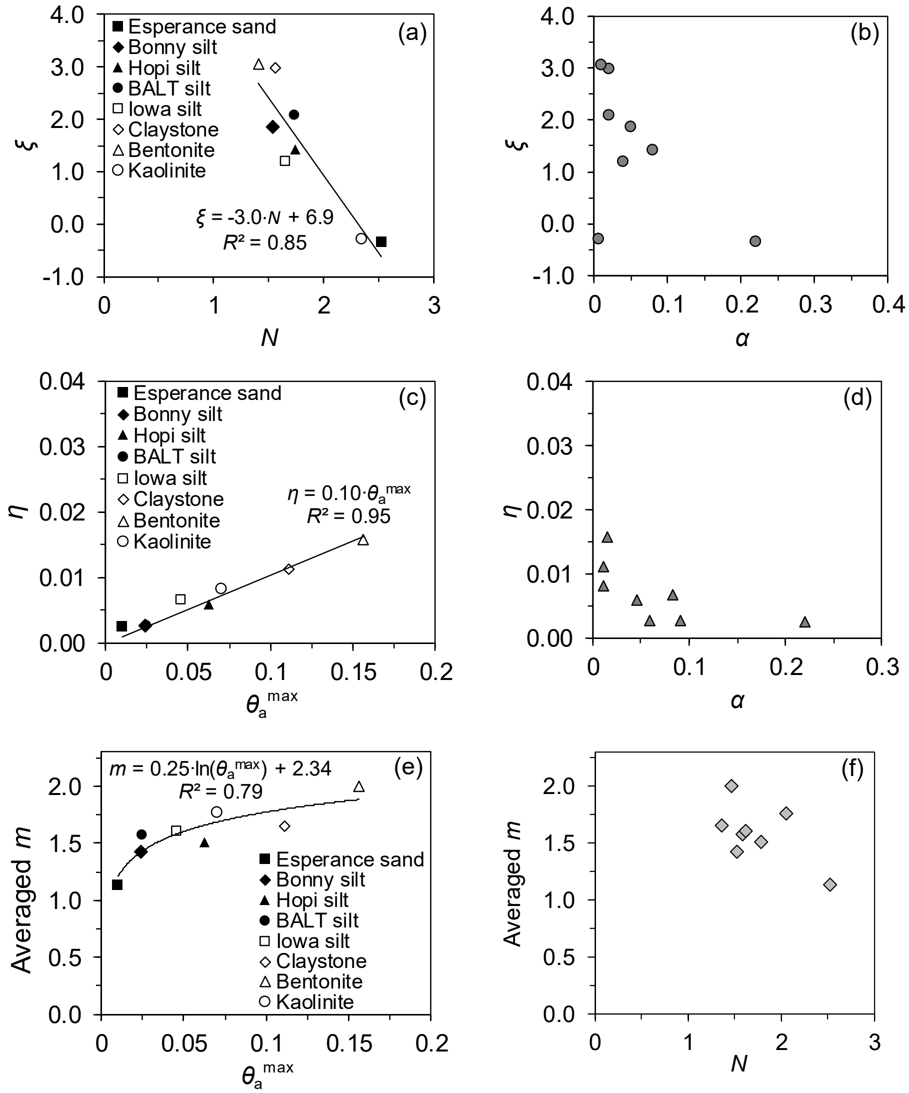
(a)
Esperance sand
Bonny silt
Hopi silt
BALT silt
Iowa silt
Claystone
Bentonite
Kaolinite
ξ = -3.0·N + 6.9
R² = 0.85
ξ
N
(b)
ξ
α
(c)
η = 0.10·θa^max
R² = 0.95
η
θa^max
(d)
η
α
(e)
m = 0.25·ln(θa^max) + 2.34
R² = 0.79
Averaged m
θa^max
(f)
Averaged m
N

Figure 8

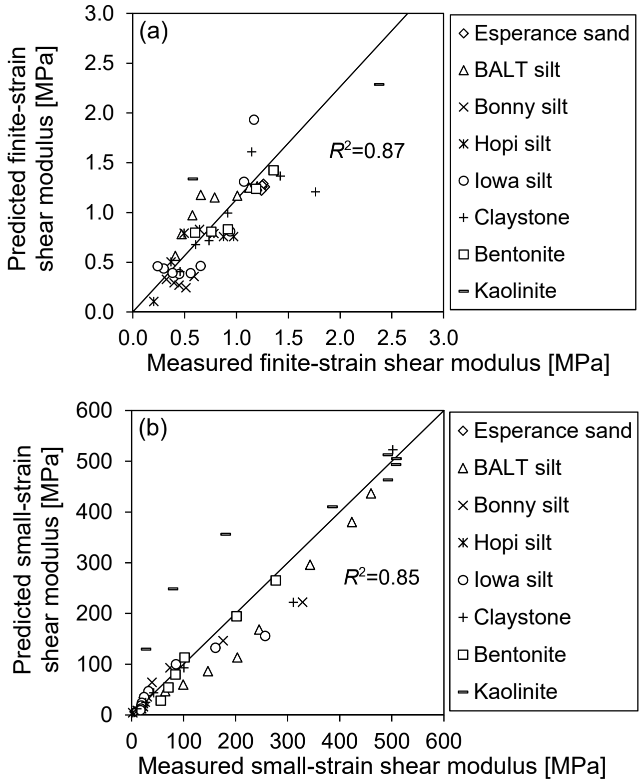

(a)
Predicted finite-strain shear modulus [MPa]
Measured finite-strain shear modulus [MPa]
R^2=0.87
0.0
0.5
1.0
1.5
2.0
2.5
3.0
Esperance sand
BALT silt
Bonny silt
Hopi silt
Iowa silt
Claystone
Bentonite
Kaolinite
(b)
Predicted small-strain shear modulus [MPa]
Measured small-strain shear modulus [MPa]
R^2=0.85
0
100
200
300
400
500
600

Figure 9

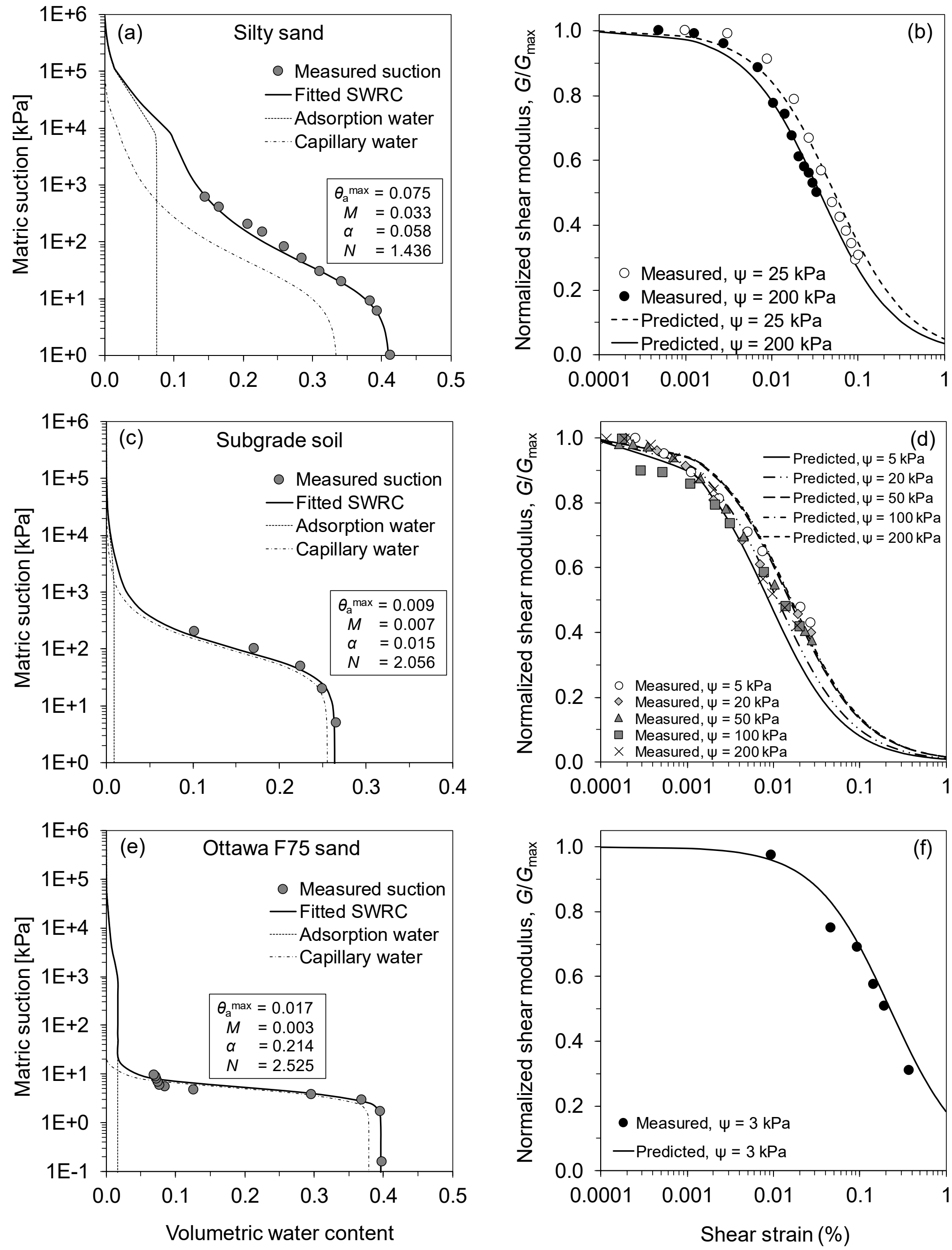

(a)
Silty sand
Measured suction
Fitted SWRC
Adsorption water
Capillary water
θ_a^{max} = 0.075
M = 0.033
α = 0.058
N = 1.436
Matric suction [kPa]
(b)
Measured, ψ = 25 kPa
Measured, ψ = 200 kPa
Predicted, ψ = 25 kPa
Predicted, ψ = 200 kPa
Normalized shear modulus, G/G_{max}
(c)
Subgrade soil
Measured suction
Fitted SWRC
Adsorption water
Capillary water
θ_a^{max} = 0.009
M = 0.007
α = 0.015
N = 2.056
(d)
Predicted, ψ = 5 kPa
Predicted, ψ = 20 kPa
Predicted, ψ = 50 kPa
Predicted, ψ = 100 kPa
Predicted, ψ = 200 kPa
Measured, ψ = 5 kPa
Measured, ψ = 20 kPa
Measured, ψ = 50 kPa
Measured, ψ = 100 kPa
Measured, ψ = 200 kPa
(e)
Ottawa F75 sand
Measured suction
Fitted SWRC
Adsorption water
Capillary water
θ_a^{max} = 0.017
M = 0.003
α = 0.214
N = 2.525
(f)
Measured, ψ = 3 kPa
Predicted, ψ = 3 kPa
Volumetric water content
Shear strain (%)